# Naturally occurring disease-related mutations in the 40-57 Ω-loop of human cytochrome *c* control triggering of the alkaline isomerisation

Oliver M. Deacon[1], Dimitri A. Svistunenko[1], Geoffrey R. Moore[2], Michael T. Wilson[1]*, Jonathan A.R. Worrall[1]*

**[1]School of Biological Science, Wivenhoe Park, Colchester, CO4 3SQ, UK. [2]School of Chemistry, University of East Anglia, Norwich Research Park, NR4 7TJ, UK.**

*To whom correspondence may be addressed:

Michael T. Wilson; wilsmt@essex.ac.uk

Jonathan A.R. Worrall; jworrall@essex.ac.uk

**ABSTRACT**

Naturally occurring mutations found in one of the two $\Omega$-loop substructures in human cytochrome $c$ are associated with low blood platelet count (thrombocytopenia). Both $\Omega$-loops participate in the formation of conformers associated with cytochrome $c$ peroxidase activity and apoptotic function. At alkaline pH values the Met80 ligand to the ferric heme iron dissociates and a lysine residue in the 71-85 $\Omega$-loop coordinates to the iron. The alkaline isomerisation has been the focus of extensive kinetic studies and it is established that a deprotonation triggers the release of the Met80 ligand ($pK_{trigger}$). A second deprotonation stabilises a pentacoordinate heme form ($pK_{a2}$). In this study, site-directed variants at the 41 and 48 positions in the 40-57 $\Omega$-loop and at the 81 and 83 positions in the 71-85 $\Omega$-loop reveal that conformational transitions in the 71-85 $\Omega$-loop, leading to the alkaline or peroxidatic conformers, are controlled by the 40-57 $\Omega$-loop. We find that the variants causing thrombocytopenia, G41S and Y48H, lower the $pK_{trigger}$ and increase $pK_{a2}$. Our results are presented in a mechanistic framework, depicted by a cube, that accounts for the pH dependencies of the equilibrium and kinetic parameters governing the alkaline transition of the native protein and $\Omega$-loop variants. The data are most consistent with the trigger for Met80 replacement by a lysine being a deprotonation within a hydrogen bonded unit that links the two $\Omega$-loops rather than an individual group. Such a proposal aligns with the entatic contribution made by the same unit in controlling the Met80-Fe(III) bond strength.

## INTRODUCTION

Mitochondrial cytochrome *c* (Cc) is a small (104 ± 10 amino acids), globular water-soluble protein with a heme group covalently attached to the polypeptide chain via thioether bonds to the cysteines of a CXXC motif [1]. Cc possesses a high degree of secondary structure, with the polypeptide fold containing five α-helices and two Ω-loops (Fig. 1). At pH 7 the heme iron is hexacoordinate with His18 and Met80 acting as the axial ligands (Fig. 1). From its re-discovery by Keilin in 1925 [2] until 1996 the role of Cc was considered to be solely that of an electron carrier in the mitochondrial respiratory chain, oscillating between its Fe(II) and Fe(III) oxidation states [1]. Now, however, it is firmly established that Cc is a multifunctional protein with roles that extend beyond its primary function of acting as an electron shuttle in oxidative phosphorylation [3]. Roles in apoptosis, redox signalling and an involvement in the mitochondrial oxidative folding machinery have been discovered [3-5]. Under apoptotic conditions, Cc complexes with the phospholipid cardiolipin (CL) to gain peroxidase activity [6], translocates into the cytosol to create the multicomponent caspase activating apoptosome [7], and enters the nucleus where it impedes nucleosome assembly [8]. This multifunctional nature of Cc arises, in part, from the flexibility of its polypeptide fold coupled with the lability of the axial Met80 ligand in the Fe(III) state. The two Ω-loops (Fig. 1) are central to the conformational flexibility of ferriCc [9, 10], and play critical roles in the altered alkaline isomerisations of medically-significant natural mutations of human Cc (hCc), as shown herein.

FerriCc has five pH dependent conformational states linked by protonation events corresponding to four distinct p$K_a$ values [11]. The hexacoordinate His/Met form, commonly referred to as the native state or state III Cc, dominates at and around neutral pH. Upon titrating state III Cc to alkaline pH, an alkaline conformer is formed (state IV Cc) [11], that results from the disruption of the Fe-S(Met80) bond and replacement of the Met80 residue as an axial ligand with a Lys residue located in the 71-85 Ω-loop; Lys 73, Lys79 or a mixture of the two depending upon solution conditions [12-14]. This conformational change in ferriCc is known as the alkaline transition and when measured under equilibrium conditions has an apparent p$K_a$ of ~ 9, depending on species and solution conditions [1, 15, 16]. From pH jump kinetic data, Davis and co-workers [17] identified an ionisable group, with a p$K_a$ of ~ 11, that, following deprotonation, is coupled to a slow conformational change that leads to the dissociation of the Met80 ligand and its replacement by a Lys. The identity of this 'triggering' ionisation has sparked intense debate in the Cc literature, but the unequivocal

identification of the trigger group (or groups) has not been satisfactorily deduced [16, 18]. Extensive spectroscopic endeavours have identified several possible groups that may serve as the trigger [3, 14, 16]. Deprotonation of the incoming ligand *i.e.* Lys73 and/or Lys79 has been considered itself to be the trigger [19], despite chemically Lys-modified Cc showing that even though the modified Lys side chains are not ionisable, the alkaline isomerisation still occurs with a small upward shift in the apparent $pK_a$ by ~0.5 to that of the unmodified protein [20, 21]. Other groups to be suggested as the trigger have included His18 [15, 22, 23], the ligand to the heme iron, Tyr67 [17, 24], an internal $H_2O$ molecule (wat166 in yeast Cc X-ray structure) [25], and a heme propionate [26, 27]. Interestingly, the latter three groups all interact with each other through an extensive H-bond network that also



**Figure 1:** X-ray structure of hCc (PDB entry 3zcf). The location of amino acids, a water molecule (grey sphere) and the resulting hydrogen bonding networks shown in red dashes, that may form a unit and have a role in 'triggering' the transition of the Met80 bound state of hCc (state III) to the alkaline conformer (state IV) as discussed in the main text. Note that the side chain of Ser47 is not shown.

includes Asn52 and Thr78 and culminates in the OH group of Tyr67 H-bonding to the Sγ atom of Met80 [28-30] (Fig. 1). Through this H-bond network, communication between the 40-57 Ω-loop and the 71-85 Ω-loop occurs (Fig. 1).

The two Ω-loops are the first structural units to unfold on Cc's unfolding pathway [31-34] with the unfolding rate of the 71-85 Ω-loop equivalent to the rate of the slow conformational change associated with Lys coordination, following Met80 dissociation in the alkaline isomerisation. The 40-57 Ω-loop unfolding rate is equal to that of an internal deprotonation rate at pH values > 10.5, an ionisation process that is not assigned to the trigger group [21, 35]. Thus, the trigger mechanism and the formation of the alkaline conformer would appear to be governed by the interplay between the two Ω-loops. Based on the relationship between the unfolding rates of the Ω-loops and key events in the alkaline isomerisation, Maity *et al.* [35] have provided a counter-view to the schemes requiring a triggering ionisation for the alkaline isomerisation. They suggest that a triggering ionisable group additional to the

Lys that becomes the replacement ligand is not needed, pointing out that since the alkaline isomerisation is an equilibrium reaction that will populate the lowest free-energy state, a pH-dependent trigger is not needed in a kinetic sense [35]. However, as we discuss later, this view has not generally found acceptance in the field with subsequent publications being based on the scheme of Davis *et al.* [17].

Under neutral conditions state III ferriCc can access a non-native conformer that has peroxidatic activity [36]. This arises due to an equilibrium between the hexacoordinate His/Met form and a pentacoordinate form in which the Met80 has dissociated [37]. The population of this conformer is exceedingly low but nevertheless sufficient for being the cause of the observed peroxidatic behaviour of Cc in the presence of $H_2O_2$ [36, 38]. Under healthy conditions this conformer assists in controlling the levels of reactive oxygen species (ROS) but during the early phases of mitochondrial apoptosis it peroxidises the phospholipid CL [6]. Three mutations in the hCc gene leading to the G41S, Y48H and A51V variants in the 40-57 $\Omega$-loop, have been discovered [39-42] and result in a rare autosomal dominant disorder, thrombocytopenia, where patients have a low platelet count resulting from increased mitochondrial apoptosis [39]. *In vitro* studies have revealed the G41S and Y48H variants have an increased population of the peroxidatic form [10, 30, 43], in the order WT < G41S < Y48H, and the apparent p$K_a$ of the alkaline transition is lowered by ~ 1 pH unit [10]. NMR studies have provided firm evidence that the increased population of the pentacoordinate form in the G41S and Y48H variants arises through extensive dynamic fluctuations in the 40-57 $\Omega$-loop and to a lesser extent in the 71-85 $\Omega$-loop [9, 10]. Thus, these findings support the notion that a dynamic coupling between these two structural units play a key role in accessing the peroxidatic conformer of hCc, as well as the formation of the alkaline conformer.

To explore further the conformational transitions that lead to the dissociation of the Met80 ligand and the switch of ligand to the alkaline conformer we have used site-directed variants in the two $\Omega$-loops of hCc. We reveal that the conformational transitions in the 70-85 $\Omega$-loop, that give rise to the alkaline and peroxidatic conformers, are controlled by the dynamics of the 40-57 $\Omega$-loop, which also regulates the p$K_a$ values of two ionisable groups that are involved in Met80 dissociation. Our results are discussed within a mechanistic framework that brings the various conformational and protonation/deprotonation events into a consistent whole, and provides a platform from which to design future experimental approaches.

**MATERIALS AND METHODS**

*Site-directed mutagenesis, over-expression and sample preparation*

The I81A, V83G and I81A/V83G variants of hCc were constructed using the Quikchange mutagenesis (Stratagene) protocol (see Supporting Information). Over-expression of wild-type (WT) hCc and all variants was carried in *E. coli* BL21(DE3) RIL cells (Invitrogen) and purified as previously described [30]. Horse heart Cc (Sigma, type VI) was used without further purification. Oxidized Cc proteins were prepared by the addition of excess $K_3[Fe(CN)_6]$, followed by removal of $K_3[Fe(CN)_6]$ and $K_4[Fe(CN)_6]$ and exchanged into a desired buffer using a PD-10 column (GE Healthcare). Protein concentration was determined with a Cary 60 spectrophotometer (Agilent) and a molar extinction coefficient ($\varepsilon$) of 106 mM$^{-1}$ cm$^{-1}$ at 409 nm. Horse heart carboxymethyl Cc (Cm-Cc), in which the heme is pentacoordinate due to the Met80 ligand being caboxymethylated and no longer able to coordinate to the heme iron, was prepared as previously described [44].

*Chemical denaturation and alkaline pH titrations*

Far-UV CD spectra at 20 $^o$C was recorded in the wavelength range 250-190 nm with an Applied Photophysics Chirascan CD spectrophotometer (Leatherhead, UK) for oxidized proteins in 10 mM potassium phosphate, 50 mM potassium fluoride pH 6.5. The stabilities of the oxidized variants were determined by titrating a 6 M stock solution of guanidine hydrochloride (GuHCl) (Fluka) to a 20 $\mu$M protein sample and the changes in molar ellipticity at 222 nm ($\theta_{222nm}$) monitored. All titrations were carried out in triplicate. The fraction unfolded ($F_u$) at any given [GuHCl] was determined [45] and the free energy of unfolding ($\Delta G_{unf}$) and dependence of $\Delta G_{unf}$ on denaturant concentration (*m* value) calculated using an equation for a two-state unfolding process [46]. The pH dependence of the 695 nm band in the UV-visible spectrum was monitored at 20 $^o$C by determining its absorbance at various values of pH for a solution of 100 $\mu$M oxidized Cc in a quartz cuvette (Hellma) with a small aliquot of $K_3[Fe(CN)_6]$ present to maintain an oxidizing environment. The pH of the buffer (20 mM sodium phosphate pH 6.0) was adjusted with microliter aliquots of 1 M NaOH and measured after each addition using a semi-micro glass pH electrode. pH titrations were repeated up to three times and with different batches of proteins. Data were fitted to a one-proton ionisation equilibrium equation to yield an apparent p$K_a$, designated herein as p$K_{695}$.

*Azide binding kinetics*

An Applied Photophysics (Leatherhead, UK) SX20 stopped-flow spectrophotometer thermostatted at $25 \pm 0.1$ °C and equipped with both photomultiplier and diode array detection systems was used to monitor the kinetics of azide ($N_3^-$) binding to the oxidized proteins. A stock solution of 2 M sodium azide (Sigma-Aldrich) were prepared in 50 mM MES pH 7.0 and diluted to the desired [$N_3^-$] with the same buffer containing 2 M NaCl to maintain the ionic strength. Reaction time-courses were taken at 420 nm with [$N_3^-$] varying between 0.08 and 2 M before mixing and 10 μM protein (before mixing). All transients were fitted to a single exponential function yielding both pseudo first-order rate constants and amplitudes. Assuming $N_3^-$ binding to oxidized Cc is an $SN_1$ mechanism, in which the hexacoordinate heme form is in equilibrium with a pentacoordinate form, the latter being the form that binds $N_3^-$, then, as outlined previously [9], equations 1 and 2 may be derived that describe the $K_{app}$ and the dependence of $k_{obs}$ for $N_3^-$ binding as a function of [$N_3^-$].

$$K_{app} = K_D\left(\frac{K+1}{K}\right) \qquad (1)$$

$$k_{obs} = \frac{(k_1 - k_{-2})[N_3^-]}{\left(\frac{k_1 + k_{-1}}{k'}\right) + [N_3^-]} + k_{-2} \qquad (2)$$

In these equations, $K = k_1/k_{-1,}$ where $k_1$ and $k_{-1}$ are the rate constants for Met80 dissociation and association respectively and $K_D = k_{-2}/k_2$, with $k_2$ the pseudo-first order rate constant for $N_3^-$ binding *i.e.* $k_2 = k'[N_3^-]$, where k' is the second order rate constant and $k_{obs}$ is ~ $k_1$ at high [$N_3^-$].

*Peroxidase assays*

Peroxidase assays of the oxidised hCc variants were carried out in the absence and presence of liposomes using $H_2O_2$ (Sigma-Aldrich) and 2,2-Azinobis(3-ethylbenthiazoline-6-sulfonic acid) (ABTS) (Sigma-Aldrich). The phospholipids 1,1',2,2'-tetraoleoyl cardiolipin (TOCL) and 1,2-dioleoyl-*sn*-glycero-3-phosphocholine (DOPC) (AVANTI Polar Lipids, USA) were mixed in a 1:1 ratio and vortexed with the appropriate amount of buffer (20 mM sodium phosphate pH 6.5) and sonicated for 5 min in a high power sonicating water bath filled with ice-cold water to give the desired stock concentration as previously described [30]. The oxidation of ABTS was monitored at 730 nm on a Hewlett-Packard 8453 diode-array spectrophotometer scanning between 190 and 1100 nm and thermostatted at 20 °C. The

reaction was initiated by the addition of 1 mM $H_2O_2$ (after 40 s) to a series of cuvettes containing 5 µM oxidized Cc and 200 µM ABTS with or without 25 µM TOCL/DOPC from a 2.5 mM stock. Using the wavelength pair 475-730 nm the slope of each trace (post-lag phase) was determined to obtain a rate in A/s. The rate of oxidized Cc turnover is reported in $s^{-1}$ obtained by dividing A/s by the product of the concertation of oxidized ABTS ($\varepsilon$ = 14 $mM^{-1}$ $cm^{-1}$) and the total protein concentration of 5 µM. All assays were carried out in triplicate with errors reported as the standard error.

*pH jump kinetics*

Various high pH buffers consisting of 50 mM KCl, 50 mM boric acid (pH 7 - 9) or 50 mM CAPS (pH 9 - 13) were prepared and stocks of oxidized proteins prepared in $H_2O$ and diluted to experimental concentrations in 50 mM KCl, to maintain ionic strength during mixing in the spectrophotometer, to a pH of ~ 7. pH jump experiments were initiated in the stopped-flow spectrophotometer by mixing protein solutions with an equal volume of high pH buffer. First order rate constants ($k_{obs}$) were obtained by fitting reaction time-courses to either a single or at pH values above 10.5 a double exponential function. Experiments were repeated in triplicate and with different batches of proteins with errors reported the standard error. All kinetic analysis was conducted using the software ProKineticist (Applied Photophysics).

*Electron Paramagnetic Resonance (EPR) spectroscopy*

Samples for EPR spectroscopy were frozen in Fluorochem SQ EPR tubes (Derbyshire, UK). To minimize the effect of slightly different tube sizes on the quantitative results, only tubes with an outer diameter of 4.05 ± 0.07 mm and an inner diameter of 3.12 ± 0.04 mm (mean ± range) were used. This ensured a low random error (1-3%) in the EPR signal intensities of a control protein solution when frozen in these selected tubes. Two methods of sample freezing for low temperature EPR measurements were used. For the slow freeze method, 250 µl of sample was dispensed into the bottom of an EPR tube and the tube placed into methanol kept on dry ice. The Rapid Freeze-Quenching (RFQ) of samples was performed by a combined use of an Update Instrument (Madison, WI) mixing machine and a home-built apparatus for freezing the ejected mixtures on the surface of a rapidly rotating aluminium disk kept at liquid nitrogen temperature. Details of the RFQ method are given in [47]. All EPR spectra were measured at 10 K on a Bruker EMX EPR spectrometer (X-band). A spherical high-quality Bruker resonator ER 4122 (SP 9703) and an Oxford Instruments liquid helium system were

used to measure the low temperature EPR spectra. To estimate absolute concentrations of the high spin (HS) and low spin (LS) ferric heme forms in the Y48H hCc EPR spectra at pH 11, a calibration experiment was performed with horse heart Cm-Cc, in a range of buffers (pH 4.5 – pH 8.5) yielding samples with variable composition of the HS and LS ferric heme forms. Experimental procedures and analysis used to determine the respective HS and LS heme concentrations are detailed in Supporting Information.

## RESULTS

*Site-directed variants of hCc used in this work*

The 71-85 Ω-loop of mitochondrial Cc is the most highly sequence-conserved region of Cc, with variation at only the 81 and 83 positions. Moving up the phylogenetic tree from yeast to mammals an increase in side chain volume at the 81 and 83 positions is observed [48]. In yeast iso-1 Cc an Ala and a Gly are found at the 81 and 83 positions, respectively, whereas in hCc an Ile and a Val, respectively, are present. Bowler and colleagues [48] have put forward the idea that steric constraints imposed by the 81 and 83 positions in mammals may influence the kinetics and thermodynamics of non-native Cc conformers. To assess the contribution of the residue volume in hCc at the 81 and 83 positions to Met80 ligand lability and the peroxidatic and alkaline isomerisation, the single I81A and V83G, and the double I81A/V83G variants were constructed. These 71-85 Ω-loop variants together with the G41S and Y48H variants located in the 40-57 Ω-loop have been used to probe the kinetic and ionisation processes associated with the alkaline isomerisation of hCc.
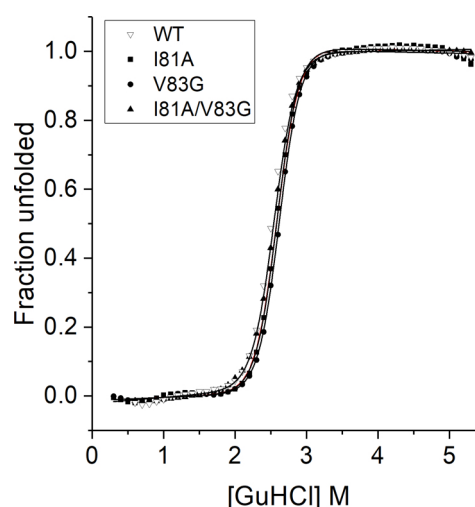


**Figure 2:** Chemical denaturation of oxidized 71-85 Ω-loop hCc variants. Data plotted as the fraction unfolded versus GuHCl concentration with solid-lines representing fits to the data using a two-state equilibrium unfolding equation. The determined thermodynamic parameters are reported in Table 1. WT hCc is included for comparison under identical experimental conditions.

*Global stability of the 81 and 83 variants*

The effect on the global stability of the 81 and 83 variants of hCc was determined by chemical denaturation using far-UV CD spectroscopy. From the data plotted in Figure 2, values for $\Delta G_{unf}$, $C_m$ and $m$ have been determined and are reported in Table 1, together with values previously reported for WT hCc under identical conditions [9, 10]. All variants display a small concomitant decrease in $\Delta G_{unf}$ and $m$ value relative to the WT protein. The most

**Table 1:** Summary of thermodynamic and kinetic parameters for WT human ferriCc and variants in the 71-85 Ω-loop determined by GuHCl denaturation and azide binding kinetics.

| | WT | I81A | V83G | I81A/V83G |
|---|---|---|---|---|
| GuHCl denaturation | | | | |
| $\Delta G_{unf}$(kcal mol$^{-1}$) | $10.65 \pm 0.55$[a] | $9.75 \pm 0.20$ | $9.95 \pm 0.10$ | $9.20 \pm 0.12$ |
| $m$ (kcal mol$^{-1}$) | $4.10 \pm 0.25$[a] | $3.80 \pm 0.10$ | $3.85 \pm 0.15$ | $3.65 \pm 0.20$ |
| $C_m$ (M) | $2.60 \pm 0.05$[a] | $2.60 \pm 0.02$ | $2.60 \pm 0.02$ | $2.55 \pm 0.02$ |
| azide binding | | | | |
| $K_{app}$ (M) | $0.31 \pm 0.03$ | $0.24 \pm 0.02$ | $0.30 \pm 0.03$ | $0.10 \pm 0.01$ |
| $k_1$ (s$^{-1}$) | $5.8 \pm 1.5$ | $14.9 \pm 6.4$ | $4.5 \pm 0.5$ | $> 70$ |
| $k_{-2}$ (s$^{-1}$) | $3.5 \pm 0.4$ | $5.9 \pm 0.5$ | $1.7 \pm 0.2$ | $3.1 \pm 0.1$ |

[a]Data taken from ref. 10.

pronounced decrease is for the double variant with a $\Delta\Delta G_{unf}$ of 1.45 kcal mol$^{-1}$. The $m$ value is a measure of the change in hydrophobic surface area that has become desolvated upon denaturation, with the decrease in $m$ values for all variants indicative of a more compact structure in the denatured state. The small magnitude of the changes observed with the 71-85 Ω-loop variants contrasts with the behaviour reported for the two variants in the 40-57 Ω-loop [10]. A $\Delta\Delta G_{unf}$ of 3.9 and 5.6 kcal mol$^{-1}$ for the G41S and Y48H variants, respectively, has been determined along with a more pronounced decrease in $m$ value, which together highlight a more significant destabilisation of the folded state in the 40-57 Ω-loop variants than for the 71-85 Ω-loop variants.

*Local stability of the 81 and 83 variants*

Local stability was tested by $N_3^-$ binding kinetics, a probe that is considered to report on the Met80-Fe(III) bond lability. Binding of $N_3^-$ to oxidized hCc follows an $SN_1$ mechanism, in which the hexacoordinate heme form (Met80-bound) is in equilibrium with a pentacoordinate form (Met80-off), the latter being the form that binds $N_3^-$. Upon mixing $N_3^-$ with oxidized hCc an optical transition occurs caused by the dissociation of the Met80 ligand from the heme iron and the binding of $N_3^-$ in its place [9]. The reaction time-course of this transition for

the 71-85 Ω-loop variants conformed to a simple exponential, as reported previously for the WT protein and the G41S and Y48H variants under the same experimental conditions [9, 10]. Over a broad range of [$N_3^-$] the normalized amplitudes of such reaction time-courses follow a simple hyperbolic binding isotherm (Fig. 3) enabling an apparent equilibrium constant ($K_{app}$) for $N_3^-$ binding to be determined using equation 1 with $K_{app}$ values reported in Table 1. Equation 1 shows that when $K$ is < 1, as here since the concentration of the pentacoordinate species is low, then $K_{app}$ is ~ $K_D/K$. With the assumption that $N_3^-$ binding to the pentacoordinate species is not directly affected by the mutation in the protein then $K_D$ will be
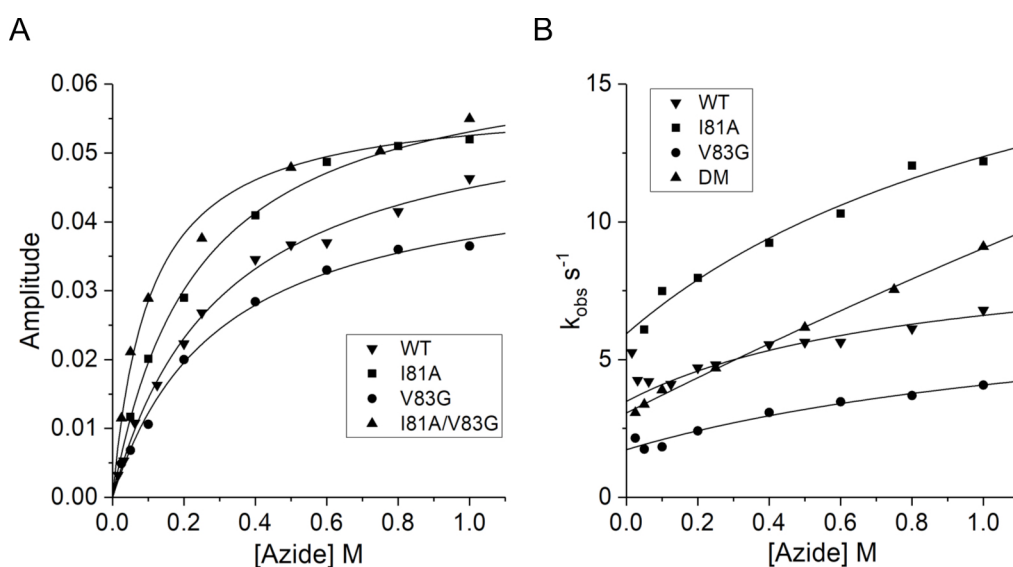


**Figure 3:** Azide binding to the oxidized 71-85 Ω-loop variants of hCc compared with data for the WT protein at pH 7.0 and 25 °C. A) Amplitude changes from the reaction time-courses obtained using stopped-flow spectroscopy at 420 nm plotted against azide concentration. Data are fitted to a hyperbolic equation to yield $K_{app}$ values reported in Table 1. B) The rate constants ($k_{obs}$) determined for azide binding with solid lines representative of fits to equation 2, to give $k_1$ and $k_{-2}$ values reported in Table 1. DM is the I81A/V83G variant.

similar for both the WT protein and variants, so that the ratio of $K_{app}$ values ($^{WT}K_{app}/^{variant}K_{app}$) reflects the ratio of $K$ values ($^{variant}K/^{WT}K$). For justification of this assumption see Supporting Information. On this basis $^{I81A/V83G}K > ^{I81A}K > ^{V83G}K = ^{WT}K$ and thus these data indicate that the pentacoordinate form of the I81A/V83G variant is more populated than in either the two single variants or the WT protein. The relationship between $k_{obs}$ and [$N_3^-$] under the conditions employed is almost linear for the 71-85 Ω-loop variants, as has previously been reported for WT hCc and the G41S and Y48H variants [9, 10]. Equation 2 predicts that the relationship between $k_{obs}$ vs [$N_3^-$] follows a hyperbola, where a curve is expected to reach a plateau (i.e. $k_1$, the Met80 ligand dissociation rate). In the present work, as in previous studies

[9, 10], it was not possible to explore a sufficiently high $[N_3^-]$ so a plateau region could not be reached. Given this, the errors in $k_1$ are large whereas $k_{-2}$ (from the $k_{obs}$ intercept and $N_3^-$ dissociation constant) have more reliable values. Nevertheless, the $k_1$ values determined in this way follow the same pattern as observed for $K$ with $^{I81A/V83G}k_1 > {}^{I81A}k_1 > {}^{V83G}k_1 = {}^{WT}k_1$ (Table 1) consistent with a more labile Met80 ligand for the double variant but a low $N_3^-$ dissociation rate constant ($k_{-2}$) and hence a low $K_{app}$.

*Peroxidase activity of the 81 and 83 variants*

Cc can act as a peroxidase, either on its own [36] or in conjunction with binding to CL in the
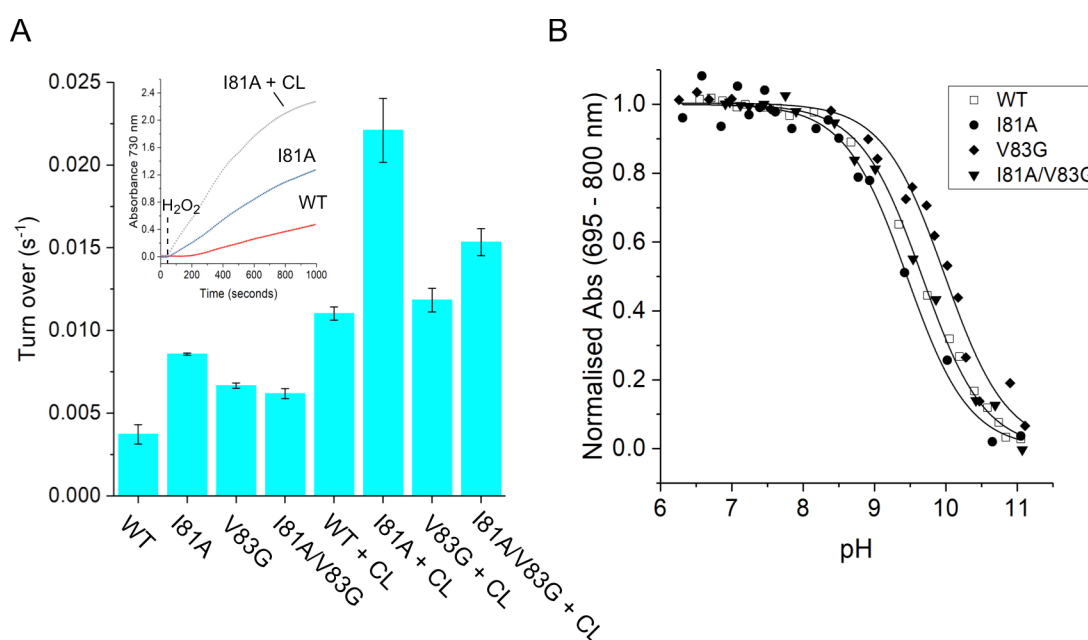


**Figure 4:** Peroxidase activity and the pH dependence of the 695 nm absorbance band for the oxidized 71-85 $\Omega$-loop variants of hCc. A) Illustrative reaction time courses (inset) for the oxidation of ABTS by oxidized hCc upon addition of $H_2O_2$ (dashed line) with (+CL) and without CL-containing liposomes. The maximum rates of ABTS peroxidation obtained from such reaction time courses for the WT and the 71-85 $\Omega$-loop variants plotted with (+CL) and without CL-containing liposomes. The error bars are the standard errors from triplicate measurements. B) The decrease of the normalised absorbance at 695 nm plotted as a function of pH for the WT and 71-85 $\Omega$-loop variants. Solid-lines are representative fits to the data using a one-proton equilibrium equation with apparent $pK_a$ values reported in Table 2.

early stages of apoptosis [6]. The peroxidase activities of the position 81 and 83 variants were tested in the absence and presence of CL liposomes. A lag phase in the peroxidase kinetics of Cc (Fig. 4A inset) has been reported [48-50] and has recently been assigned to the oxidative activation of a pre-catalytic form leading to the formation of oxidised proteoforms with high peroxidatic activity [51]. These species consist of a pentacoordinate heme form, in which the

Met80 ligand is dissociated and subsequently becomes oxidised, together with an oxidised Tyr67 and carbonylated Lys72/73 [51]. It is noteworthy that the 71-85 $\Omega$-loop variants in the absence of CL-liposomes do not display the distinct lag phase after addition of $H_2O_2$ as seen in the WT hCc (Fig. 4A inset). The complete absence of a lag phase has also been observed with the G41S and Y48H variants [10, 30]. The 71-85 $\Omega$-loop variants all display increased peroxidase activity relative to the WT hCc in the absence of CL-liposomes, of the order I81A > V83G = I81A/V83G > WT. As expected, in the presence of CL-liposomes the peroxidase activity is further enhanced, particularly for the I81A variant with an order of activity, I81A > I81A/V83G > V83G = WT. It is noteworthy that whilst decreasing the residue volume at the 81 and 83 positions leads to a peroxidase rate increase compared to the WT protein, the enhancement is considerably lower than with the G41S and Y48H variants, where a 3 and 7-fold increase, respectively, relative to the WT hCc is observed [10].

*Equilibrium alkaline isomerisation of the 81 and 83 variants*

The contribution of the amino acid at the 81 and 83 positions in hCc to the formation of the alkaline conformer was tested under equilibrium conditions. The 695 nm band in the absorption spectrum of Cc reports on the presence of the Met80(S$\gamma$)-Fe(III) heme bond [1, 52]. On increasing the pH the 695 nm band decreases in intensity due to a transition involving dissociation of a single proton that results in Met80 dissociation and its replacement by a Lys residue present in the 71-85 $\Omega$-loop, creating the state IV species [11]. The apparent $pK_a$ of this alkaline transition is the parameter determined in these experiments. The I81A variant does not alter the apparent $pK_a$ relative to the WT protein (Table 2), but an increase of 0.8 pH units is observed for the V83G variant (Table 2). In contrast the double I81A/V83G variant has a $pK_a$ value 0.4 pH units higher than the WT but notably 0.4 units lower than the V83G variant giving an apparent $pK_a$ pattern of V83G > I81A/V83G > I81A = WT. Thus, the $pK_a$ of the I81A/V83G variant is an example of biochemical epistasis, whereby the V83G variant has a different effect in combination with the I81A variant than on its own. A shift to a higher $pK_a$ for the V83G and I81A/V83G variants is consistent with a destabilisation of the alkaline state relative to the WT protein. In contrast the G41S and Y48H variants in the 40-57 $\Omega$-loop have apparent $pK_a$ values lower by ~ 1 pH unit than the WT protein, and are thus consistent with a stabilisation of the alkaline form relative to WT hCc (Table 2).

*Kinetics of the alkaline transition below pH 10 for the $\Omega$-loop variants*

To elucidate the mechanistic features of the transition to the alkaline conformer, and to assess the effect of the respective variants in the 71-85 and 40-57 $\Omega$ loops have on this, the kinetics of the transition were investigated using a series of stopped-flow pH jump experiments. The kinetics of the alkaline transition in Cc is generally discussed in terms of the simple model [17] (Scheme 1) in which deprotonation of a group, that is yet to be identified and is termed the trigger, initiates a conformational change that leads to the substitution of the Met80 ligand by a Lys residue from the 71-85 $\Omega$-loop.

$$^hCc\text{-}H_{trig} \underset{}{\overset{-\,H^+}{\rightleftarrows}} {}^hCc \underset{k_{b1}}{\overset{k_{f1}}{\rightleftarrows}} {}^hCc\text{-}Lys$$
$$K_{a1} \qquad\qquad K_c$$
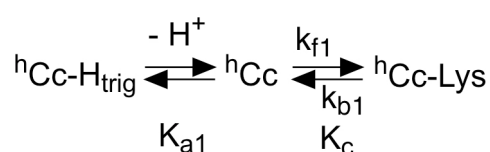
Scheme 1

In Scheme 1, $^hCc\text{-}H_{trig}$ depicts the His/Met hexacoordinate protein with the trigger protonated, $^hCc$ the His/Met hexacoordinate protein with the trigger deprotonated, and $^hCc\text{-}Lys$ a hexacoordinate conformer of Cc having undergone a conformational change that includes replacement of Met80 as the axial ligand by a Lys residue. $K_{a1}$ and $K_c$ are equilibrium constants for the protonation/deprotonation and the conformational change, respectively, and $k_{f1}$ and $k_{b1}$ are the forward and backward rate constants associated with the second step, respectively. On jumping from pH 7.0 to higher pH values, optical transitions for WT hCc consistent with those reported previously for horse and hCc were observed [21, 53, 54]. In the pH range 7.0 to 10.0, WT hCc along with all variants displayed a single spectral transition, with the Soret band blue-shifted (Fig. 5A) and the 695 nm band bleached. This transition could be adequately fitted to a single exponential phase (*inset* Fig. 5A), although distribution of residuals indicated the possible presence of minor components, as has been previously discussed [54]. The rate constant ($k_{obs1}$) of this single exponential increased as expected with increasing pH [17]. This behaviour is shown in Figure 5B in which, for clarity, log $k_{obs1}$ is plotted as a function of pH. Given that the deprotonations of the trigger are very fast, the model in Scheme 1 yields equation 3, relating $k_{obs1}$ to $K_{a1}$, $k_{f1}$ and $k_{b1}$

$$k_{obs1} = k_{b1} + k_{f1}\left(\frac{K_{a1}}{K_{a1}+H^+}\right) \qquad\qquad (3)$$

Equation 3 indicates that $k_{obs1}$ follows a simple titration curve in which $k_{obs1}$ takes the value $k_{b1}$ at low pH and $k_{b1} + k_{f1}$ at high pH values, *i.e.* $k_{obs1}$ increases with pH. The data plotted in
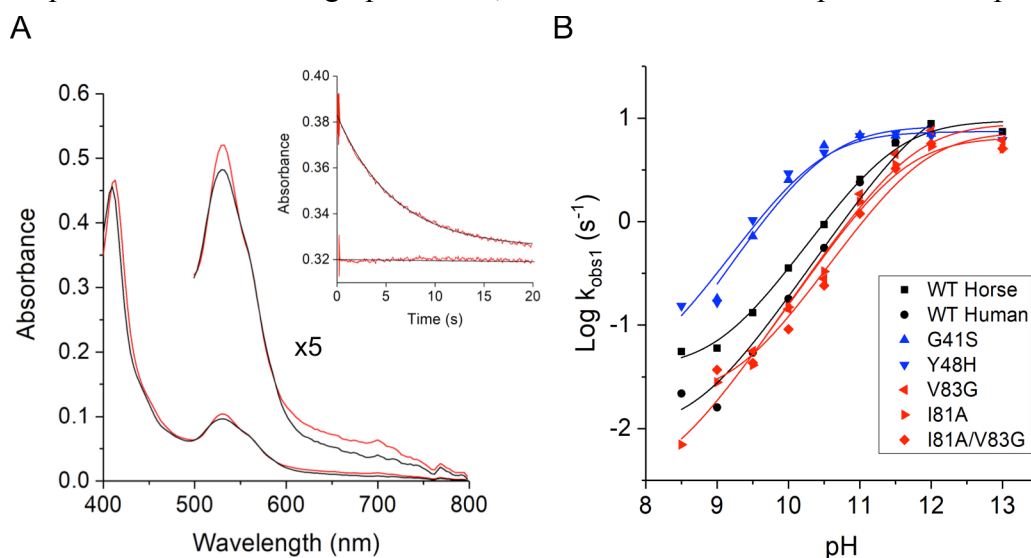


**Figure 5:** pH jump kinetics of the slow phase of ferric hCc and variants. A) Optical transitions observed from stopped-flow spectroscopy on mixing oxidised WT hCc (pH 7) with an equal volume of a pH 10 buffer. The red line represents the ferric hexacoordinate form (state III) at $t = 2.5$ ms and the black line corresponds to the hexacoordinate alkaline form (state IV) at $t = 20$ s. The spectral region between 500-800 nm has been magnified 5-fold. Inset shows a typical reaction time-course at 420 nm (red) together with the corresponding fit to a single exponential function (black line) with residuals of the fit shown. B) The pH dependence of $k_{obs1}$ for the slow phase of the alkaline transition. The lines are fits to the logarithmic transformation of equation 3 to yield the p$K_{a1}$ (Table 2). Plots representing amplitudes are presented in Supporting Information.

Figure 5B have been fitted with equation 3 to yield the p$K_{a1}$ of the trigger, with values reported in Table 2. For the 81 and 83 variants, the p$K_{a1}$ values all cluster around the value determined for the WT hCc and horse Cc (the latter used as a control in this work owing to the extensive literature on the pH jump kinetics of this protein [21, 53]). In contrast, the G41S and Y48H variants reveal a lower p$K_{a1}$ by > 1 pH unit (Table 2). Thus, the 40-57 Ω-loop variants strongly influence the deprotonation behaviour of the trigger, whereas the 71-85 Ω-loop do not. Furthermore, as the decrease observed for the G41S and Y48H variants is reflected in the apparent p$K_a$ of the alkaline transition (Table 2) [10], the value of $K_c$ must remain largely unchanged at ~$10^2$ (p$K_c = -2$ so $K_c = 100$). This follows from the relationship, p$K_a$ = p$K_{trigger}$ + p$K_c$, stemming from Scheme 1. We are not able to determine $K_c$ directly from our data (Fig. 5B) because the $k_{b1}$ values are small (typically > 0.03 s$^{-1}$), and either measured from small amplitude changes at an end of the titration (WT protein and the 81 and 83 variants) or derived by extrapolation of the data to pH values much lower than explored in

the data set (G41S and Y48H). However, $k_{fl}$ values are determined with a reasonable level of accuracy (Table 2). For horse Cc the $k_{fl}$ value under our conditions correlates well with previous kinetic studies [21, 53], with the $k_{fl}$ values for the variants and the WT hCc all on the same order of magnitude. This similarity in $k_{fl}$ values is consistent with similar $K_c$ values.

**Table 2:** Summary of parameters determined for the alkaline transition of horse heart and human ferricCc and variants.

| | WT horse | WT human | I81A | V83G | I81A/V83G | G41S | Y48H |
|---|---|---|---|---|---|---|---|
| $pK_{695}$ | $9.2 \pm 0.1$ | $9.3 \pm 0.2^a$ | $9.4 \pm 0.2$ | $10.1 \pm 0.1$ | $9.7 \pm 0.1$ | $8.5 \pm 0.2^a$ | $8.4 \pm 0.1^a$ |
| $pK_{a1}$ ('trigger') | $11.5 \pm 0.1$ | $12.0 \pm 0.4$ | $11.6 \pm 0.1$ | $11.7 \pm 0.2$ | $11.8 \pm 0.2$ | $10.5 \pm 0.1$ | $10.4 \pm 0.2$ |
| $k_{fl}$ (s$^{-1}$) | $9.5 \pm 1.2$ | $17 \pm 13$ | $6.5 \pm 1.6$ | $8.9 \pm 3.4$ | $7.3 \pm 2.5$ | $8.4 \pm 1.3$ | $7.4 \pm 1.4$ |

[a]Data taken from ref. 10

*Kinetics of the alkaline transition above pH 10 for the Ω-loop variants*

At higher pH values (> 10) a second rapid phase in addition to the slow phase ($k_{obs1}$) was
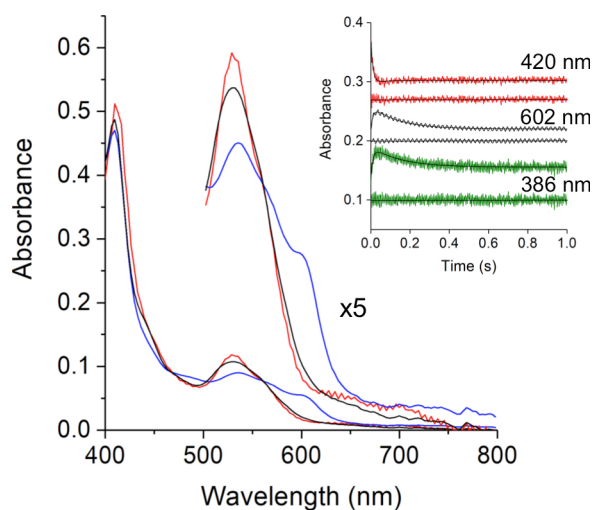


**Figure 6:** pH jump kinetics of the fast phase of the Y48H variant of hCc at pH > 10.5. Optical transitions from stopped-flow spectroscopy on mixing oxidised Y48H hCc (pH 7) with an equal volume of a pH 11 buffer. The red line represents the ferric hexacoordinate protein (state III) at $t = 3.5$ ms, the blue line reflects the HS pentacoordinate form at $t = 36$ ms and the black line reflects the final hexacoordinate alkaline form (state IV) at $t = 1$ s. The spectral region between 500-800 nm has been magnified 5-fold. Inset shows the reaction time-courses at three wavelengths with the residuals of the corresponding fit to a double exponential shown. Plots representing amplitudes are presented in Supporting Information.

observed for the WT protein and all Ω-loop variants, consistent with previous reports for horse Cc [21, 53, 55] and hCc [54] (*inset* Fig. 6). The rate constant ($k_{obs2}$) is associated with the formation of a transient spectrum characteristic of a HS ferric heme species having a prominent band at 600 nm and possessing long wavelength features that obscure the bleaching of the 695 nm band at some pH values (Fig. 6) [21, 53]. Thereafter, the spectrum decays to the final LS spectrum typical for ferriCc at high pH in which a Lys substitutes for Met80 as the sixth ligand (Fig. 6). It is notable that this HS intermediate is more highly populated in the Y48H and G41S variants than in WT hCc. The rate constant ($k_{obs2}$) for this fast phase was also found to be pH dependent for all proteins studied (Fig. 7A and B). For WT hCc the $k_{obs2}$ decreases with increasing pH in the range 10 to 11.5 and takes values similar to horse Cc (Fig. 7A). This behaviour can be represented by Scheme 2 and has been suggested to arise from a coupling between a conformational change that exposes a group that then undergoes deprotonation leading to the stabilisation (or facilitation) of the HS heme species [21].

$$^{h}Cc\text{-}H \underset{k_{b2}}{\overset{k_{f2}}{\rightleftarrows}} {^{P}Cc\text{-}H} \underset{K_{a2}}{\overset{-\,H^+}{\rightleftarrows}} {^{P}Cc}$$
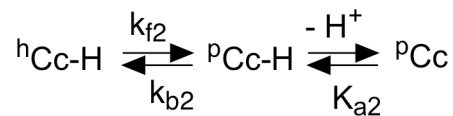
Scheme 2

In Scheme 2, $^{h}Cc$-H (hexacoordinate His/Met) and $^{P}Cc$-H (pentacoordinate) represent the non-exposed and exposed group, respectively, and $^{P}Cc$ the deprotonated HS heme form. The model presented in Scheme 2 leads to equation 4 to relate $k_{obs2}$ with $k_{f2}$, $k_{b2}$ and $K_{a2}$ for the formation of the HS heme species.

$$k_{obs2} = k_{f2} + k_{b2}\left(\frac{H^+}{(K_{a2}+H^+)}\right) \tag{4}$$

Equation 4 predicts that $k_{obs2}$ decreases with increasing pH, as observed in Fig. 7A for horse Cc and WT hCc. Although the data are not sufficient to provide a clear $pK_{a2}$ with confidence an estimate of $\leq 10$ may be surmised from the shape of the relevant lines (Fig. 7A). In contrast the G41S and Y48H variants show very different behaviour, in that the $k_{obs2}$ for production of the HS heme species increases with increasing pH and is readily observed at pH values > 10 (Fig. 7A). These data may be fitted to a one-proton ionisation equilibrium equation to yield a $pK_{a2}$ of 11.1 ± 0.2 for the exposed group. Taken together these data imply

that deprotonation precedes the conformational change that leads to the dissociation of the Met80 ligand from the heme iron of the G41S and Y48H variants. Hence the mechanism of the alkaline isomerisation for the 40-57 $\Omega$-loop variants, at least in terms of the appearance of intermediates on the pathway, is different to that of WT hCc and the 71-85 $\Omega$-loop variants.

In contrast the 81 and 83 variants show different behaviour in $k_{obs2}$ compared to either
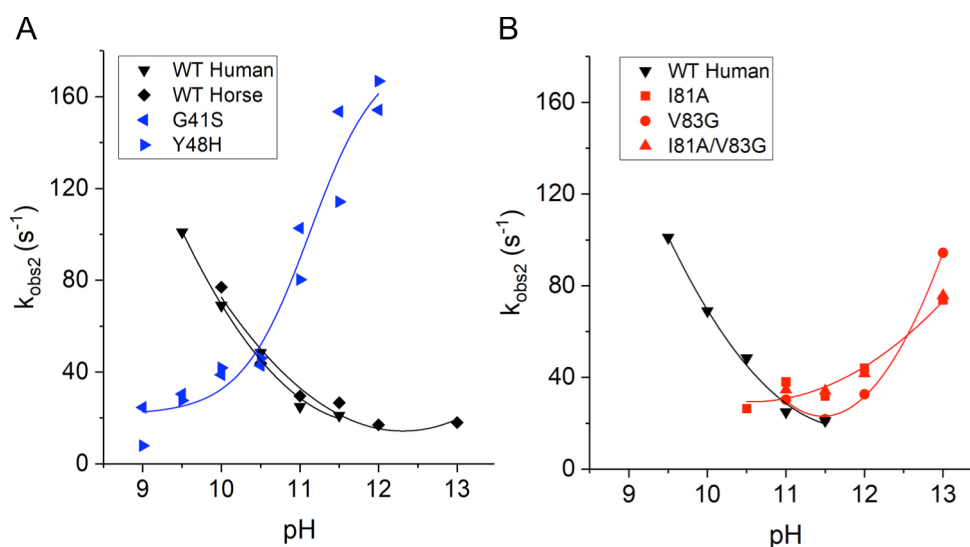


**Figure 7:** The pH dependence of $k_{obs2}$. The $k_{obs2}$ values for WT hCc, horse Cc, the G41S and Y48H variants of hCc A) and the 70-85 $\Omega$-loop variants B) plotted as a function of pH. The lines through the data points for hCc, horse Cc and the 70-85 $\Omega$-loop variants is to indicate the trends in the data. The blue line in A is a fit to a one-proton equilibrium equation to yield an apparent p$K_a$. This fit is to the combined results of the two 40-57 $\Omega$-loop variants.

the WT or the 40-57 $\Omega$-loop variants. Firstly, from pH values 7 to 10 no HS heme species was observed. At pH values > 10.5 the HS heme species for the 81 and 83 variants is detected with $k_{obs2}$ values increasing with increasing pH up to pH 13 (Fig. 7B). Given the high pH at which we observe this increase in $k_{obs2}$ we suggest that the process through which a HS heme species is generated is related to a more general denaturation of the protein rather than the process termed the alkaline isomerisation.


*EPR spectroscopy to determine the population of the HS heme species*

EPR spectroscopy was used to verify that the intermediate species seen in the pH jump experiments was indeed a HS heme form. Based on the optical spectroscopy, a higher population of the HS species is found in the 40-57 $\Omega$-loop variants and therefore the Y48H variant was selected for EPR experiments. At pH 7, slow freezing the Y48H variant produces a HS heme species, ($g_1$ = 6.03, $g_2$ = 5.67), which is absent in the rapid freeze-quenched

(RFQ) sample (Fig. 8, A and B). There is also a difference in the intensities of the LS ferric heme signals ($g_1 = 3.05$, $g_2 = 2.23$) in the slow frozen and RFQ samples. These results
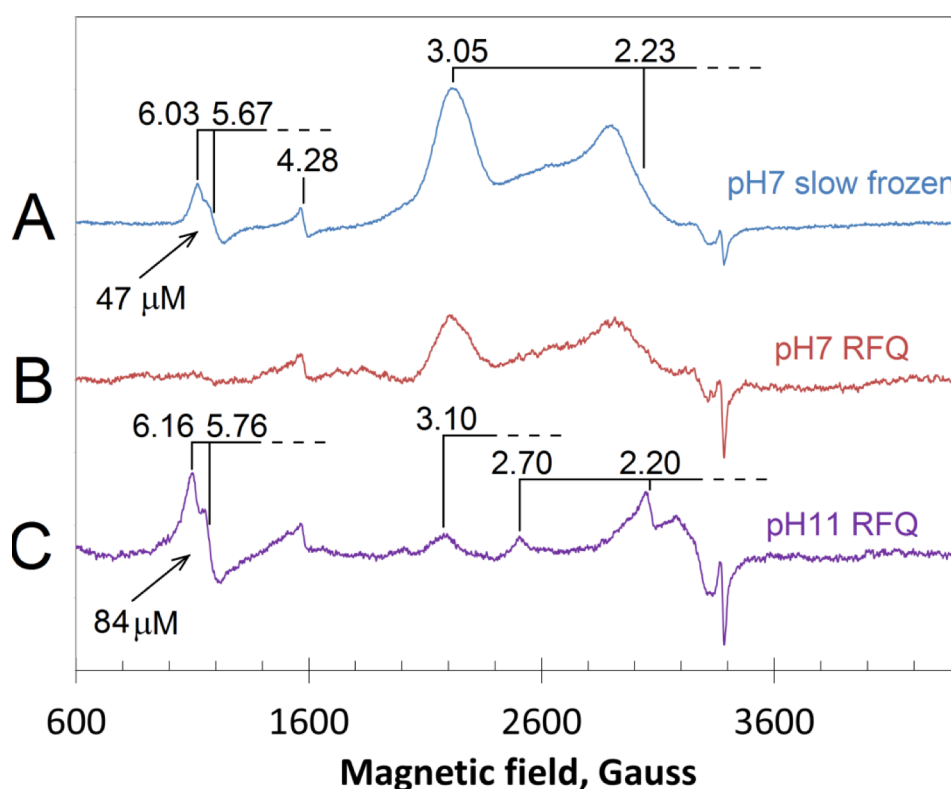


**Figure 8:** The effect of the pH jump (pH 7 to pH 11) on the LS and HS ferric heme states in the Y48H variant of hCc determined by EPR spectroscopy. Final concentration of protein after mixing was 200 μM. A) EPR spectrum of protein at pH 7 mixed with an equal volume of the pH 7 buffer followed by slow freeze, B) protein at pH 7 mixed with an equal volume of the pH 7 buffer and RFQ at 50 ms, and C) protein at pH 7 mixed with equal volume of the pH 11 buffer and RFQ at 50 ms. The concentration of the HS ferric heme form (indicated on the figure) was estimated from comparison with the acid-alkaline transition of the HS and LS forms in Cm-Cc (see Supporting Information). The EPR spectra were measured at 10 K with the instrumental conditions the same as specified in Figure S3. To make all three spectra directly comparable, spectrum A was multiplied by a factor of 0.45 to account for imperfect packing of the freeze-quenched icicles in the EPR tubes.

highlight the effect different regimes of freezing (slow or fast) have on the quantities of quenched species that have been in dynamic equilibrium in the liquid phase just before freezing. The RFQ of the Y48H variant at 50 ms after the pH jump (pH 7 to 11) results in an EPR spectrum with a notable intensity of the HS ferric heme signal ($g_1 = 6.16$, $g_2 = 5.76$), and a significantly decreased LS ferric heme signal (as evident from its $g_1 = 3.10$ component, Fig. 8, B and C). The absolute concentrations of the HS ferric heme forms in the RFQ pH 11 EPR spectrum (84 μM, Fig. 8C), was determined from the Cm-Cc calibration experiment as

19

described in the Supporting Information. This concentration constitutes approximately 42 % of the total heme concentration in the Y48H variant.


**DISCUSSION**

Reducing the side chain volume of the residue at position 81 and 83 in the 71-85 $\Omega$-loop of hCc results in only a small increase in peroxidase activity. The double I81A/V83G variant has less peroxidase activity than the single I81A variant suggesting that replacing a Val at position 83 with the smaller side chain volume of a Gly compromises formation of the peroxidatic pentacoordinate state in the absence of the Ile81. This is consistent with studies of other proteins showing it is easier to accommodate a hole in a protein than a bulkier group [56]. In the presence of CL, the compromising role of a Gly at the 83 position is somewhat relieved in the double variant, suggesting that there are differences in the peroxidatic conformer formed in the absence and presence of CL, consistent with CL binding causing a change in conformation of ferriCc. Nevertheless, the minimal enhancement of peroxidase activity observed with the 71-85 $\Omega$-loop variants contrasts sharply with the up to 7-fold increase in activity for the 40-57 $\Omega$-loop variants [10]. Thus, the ferric G41S and Y48H variants must have higher concentrations of the pentacoordinate states, consistent with our $N_3^-$ binding studies (Table 1). Thus, in hCc the side chain volumes at the 81 and 83 positions in the 71-85 $\Omega$-loop do not materially regulate the peroxidase activity, results consistent with a recent study in which the Ala81 and Gly83 residues in yeast iso-1 Cc were switched for Ile and Val, respectively, and showed the reciprocal behaviour [57].

Determining the $pK_{695}$ value and employing kinetics to monitor the binding of exogenous ligands, such as $N_3^-$, to ferriCc are widely considered to give information on the lability of the Fe(III)-S(Met80) bond. The trend in $pK_{695}$ values, V83G > I81A/V83G > I81A = WT differs from the trend observed in peroxidase activity (Fig. 4A), most notably in that I81A has the highest activity. Furthermore, from $N_3^-$ binding kinetics, the determined affinities for $N_3^-$ binding and Met80-off rates ($k_1$) both follow the same trend *i.e.* I81A/V83G > I81A > V83G = WT, implying that the double variant induces a more labile Met80 ligand with possibly greater ease of access for the $N_3^-$ to bind the ferric heme, whereas the V83G variant is identical to the WT protein. These results appear inconsistent with the trend in peroxidase activity and $pK_{695}$ values. However, these various probes used to explore conformational changes around the heme - $pK_{695}$, $N_3^-$ binding and peroxidase activity - report on related but different aspects of the heme protein dynamic. For example, in comparing $N_3^-$

binding and peroxidase activity, where in both cases a ligand binds to the heme, it may be expected that subtle differences are exhibited between the different variants based on the physicochemical nature of the incoming ligand; $H_2O_2$, a small neutral molecule, *vs* $N_3^-$, a rigid linear anion). Whilst the I81A variant displays the greater peroxidase activity, the I81A/V83G variant has the greater facility to bind $N_3^-$, implying that while I81A has a pentacoordinate form, it is not easily accessible to $N_3^-$, whilst it is easily available to $H_2O_2$. Conversely, the high affinity of $N_3^-$ for the I81A/V83G variant is seen to arise from a low $k_{-2}$ (relative to the high Met80 off rate (see also Supporting Information)). This may be a consequence of $N_3^-$ being accommodated better in this variant which has the bulky groups removed. In addition, the p$K_{695}$ value reflecting the removal of the coordinating Met80 does not necessarily give information on the population of the pentacoordinate form which is a prerequisite for peroxidase activity. Thus, we conclude that for I81A, although the p$K_{695}$ value is close to that of the WT protein the population of the pentacoordinate form at equilibrium is greater. There appears therefore to be modulation of the global effects of loop dynamics by bulky residues near Met80.

A complete description of the pH dependencies of the equilibrium and kinetic parameters governing the alkaline transitions in hCc, requires adoption of a model that incorporates sufficient steps to provide a mechanistic description. There must be a minimum of two deprotonation steps (both fast), one for the trigger and one responsible for the transition to the HS heme species, as well as a conformational equilibrium between hexacoordinate (Met80-on) and pentacoordinate (Met80-off) forms. In addition, one must consider Lys binding to the pentacoordinate form to give the final hexacoordinate alkaline conformer (state IV). The simplest model that satisfies these requirements and is consistent with mechanisms given in Schemes 1 and 2, is depicted in Figure 9, where the various forms of ferriCc are placed at the corners of a cube. The edges of the back and front faces of the cube represent the protonation/deprotonation equilibria, horizontal edges refer to the trigger while vertical edges to the second ionisable group responsible for the appearance of the HS form (Fig. 9). The edges linking the back to the front face represent the conformational equilibria (*i.e.* hexa- to pentacoordinate). Also indicated are possible steps for Lys binding to the species populating the pentacoordinate face. Starting from WT Cc in state III (back left hand corner of the cube, H-$^h$Cc-H$_{trig}$) where both ionisable groups are protonated and the Cc is hexacoordinate, Scheme 1 follows the grey arrows where deprotonation of the trigger precedes conformational change to a pentacoordinate form (H-$^p$Cc), which subsequently binds Lys. All the variants studied follow this pathway, the p$K_{trig}$ is however variant

dependent, being > 1 pH unit lower in the G41S and Y48H variants (Table 2). The formation of the observed HS heme species results from a conformational change preceding deprotonation (Scheme 2). Within the cube, this is depicted by the silver arrows. A minor population of the pentacoordinate form at pH 7 (H-$^P$Cc-H$_{trig}$), the existence of which is inferred from N$_3^-$ binding experiments [9], is stabilised by deprotonation of the second group. Thus, the observed HS form is either $^P$Cc-H$_{trig}$ or $^P$Cc (or both), with both these species decaying through Lys binding (Fig. 9). The 71-85 $\Omega$-loop variants do not deviate from this

mechanism and therefore the residue volume at the 81 and 83 positions do not alter this ionization process or the route in the cube that can be taken to the HS form. In contrast, for the 40-57 $\Omega$-loop variants, it is observed that the pH dependence of $k_{obs2}$ reflects a mechanism in which deprotonation precedes conformational change (Fig. 7A). As the p$K_{a2}$
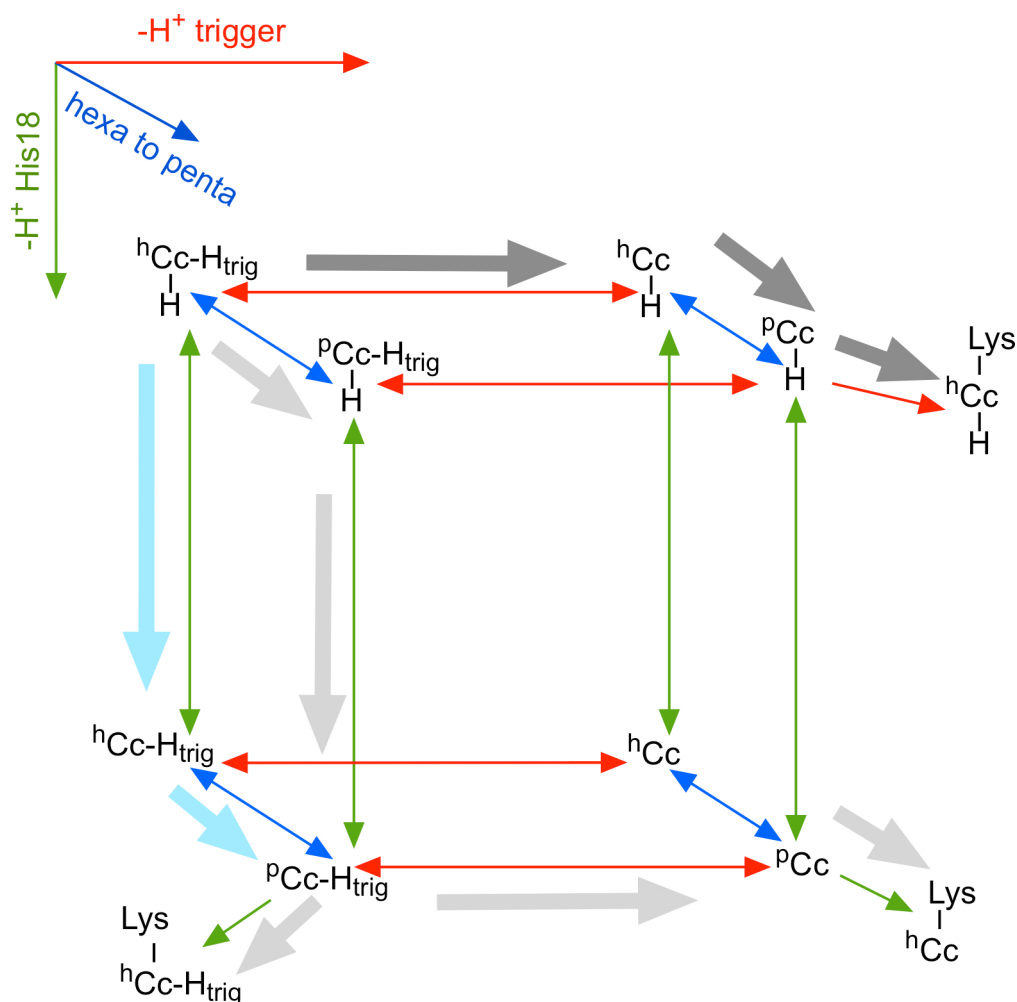


**Figure 9:** Mechanistic pathway linking deprotonation and conformational changes in hCc. The three dimensions of the cube represent two deprotonations ("trigger" and another group possibly His18, see main text) and a conformational change leading to Met80 dissociation. The front face of the cube shows the pentacoordinate forms (denoted by $^{P}$Cc) which in principle can bind an amino group donated by a Lys residue. The likely routes through the mechanistic framework are indicated by the larger grey and silver arrows, for the WT protein and the 71-85 $\Omega$-loop variants, with the pale blue arrows indicating the route for the G41S and Y48H variants to populate the $^{P}$Cc-H$_{trig}$ species, which then follows the silver arrows. See text for further details.

value of 11.1 is higher than the p$K_{trig}$ for the G41S and Y48H variants (Table 1) it seems unlikely that the same ionising group is responsible for these two p$K_{a}$ values. Also, it is difficult to construct a model in which a single trigger group is simultaneously responsible

for two apparently quite different transitions, namely the slow (alkaline transition) and fast (formation of HS) processes. Taking this view, and by not complicating the model further, we conclude, that the enhanced dynamics of the 40-57 $\Omega$-loop observed in the G41S and Y48H variants makes the second group available for deprotonation. In these proteins then, the initial step takes H-$^h$Cc-H$_{trig}$ to $^h$Cc-H$_{trig}$ (pale blue arrows Fig. 9) and thereafter the conformational change leads to the pentacoordinate HS species that we observe.

Having devised the cube to depict the kinetics of the alkaline transition, what may be the titratable groups responsible for the alkaline transition and the transition to the HS state? Several possibilities in respect to the nature of the trigger have been extensively discussed in the literature [3, 14, 16, 18, 58]. Whilst the present study does not provide the definitive answer to the nature of the trigger, our results do further illuminate the properties of the trigger and how these relate to the mechanism of the alkaline transition as portrayed in the cube (Fig. 9). We consider first the alkaline transition which leads to the substitution of Met80 by a Lys and has an apparent equilibrium p$K_a$ of ~9 [16] with a triggering ionisation p$K_{trig}$ of ~12. The G41S and Y48H hCc variants have a lower p$K_{trig}$ (Table 2) and have enhanced dynamics in the 40-57 $\Omega$-loop compared with the WT protein [9, 10]. The pH jump kinetics for the T49V variant of horse Cc paints a similar picture, in that the triggering p$K_a$ is lowered with respect to WT horse Cc to 9.1 [59]. Thr49 hydrogen-bonds (H-bonds) to HP-6 which in turn H-bonds to Thr78 (Fig. 1). Disrupting communication to the heme propionate-6 (HP-6) in the T49V variant has a more severe effect on the triggering p$K_a$ than either of the disease variants and accounts for the apparent p$K_a$ of 7.0 [59]. From a functional perspective, the disease variants do not lower the triggering p$K_a$ sufficiently for Lys coordination to dominate at neutral pH, thus ensuring a balance of Met80 coordination needed for electron transfer and the pentacoordinate form for pro-apoptotic peroxidase activity. Moreover, it is further apparent that distant H-bonding networks communicating with the Met80 ligand and the 40-57 $\Omega$-loop are important in controlling the Met80 dissociation. Solomon and co-workers [60, 61] have reported that the strength of the Fe(III)-S$\gamma$(Met80) bond is enhanced by an entatic contribution of the protein derived from a H-bonding network that includes the coordinating Met80, Tyr67/wat166, Asn52 and Thr78. We may add to this network the heme propionate groups, which serve to communicate with the 40-57 $\Omega$-loop (Fig. 1). Thus, an attractive proposition is that the loss of a single proton from within this linked H-bonded unit can disrupt it, weakening the Fe(III)-S$\gamma$(Met80) bond. The p$K_a$ of this deprotonation must be high because of the H-bonded nature of the network. In the case of the G41S and Y48H variants, the substitutions in the 40-57 $\Omega$-

loop alter the H-bond network to HP-7 and the Asn52, and may lower the p$K_a$ of this stabilising unit and hence lower the triggering p$K_a$ and thus the apparent p$K_a$ of the alkaline transition.

Our suggestion that it is a H-bonded unit that provides the triggering ionisation rather than an individual group has not been made previously and it neatly brings together a considerable body of experimental data. Early NMR and X-ray crystallographic data first indicated that the network involving HP-7 was dynamic in solution continually being disrupted and reformed [1]. Subsequent site-directed mutagenesis experiments have revealed that the network is altered in the N52I and N52I/Y67F variants of yeast iso-1 ferriCc, particularly with respect to the location of wat166 [29], and the Y67H and Y67R variants of yeast ferriCc behave similarly to the G41S and Y48H variants of hCc in having a more labile Fe(III)-Sγ(Met80) bond and enhanced peroxidase activity [62]. Moreover, pH-jump stopped-flow FT-IR data shows that a HP substituent ionises as well as a Tyr residue during the alkaline isomerisation [63, 64]. Several studies using site-directed variants of the alkaline ligands (*i.e.* Lys) in yeast iso-1 Cc have provided further evidence to indicate a role of a HP ionization in modulating the kinetics of the alkaline transition [65, 66].

Through substitution of coordinating Lys residues (73 or 79) with His or Ala residues in yeast iso-1 Cc, Bowler and colleagues [58, 65, 66] have highlighted that multiple ionisations are involved in the kinetics of the alkaline transition; a concept close to our proposal of an ionisation within a H-bonded unit constituting the trigger. Furthermore, the His substitutions reveal that ionisation of the incoming ligand can have a prominent kinetic role [58, 65, 66]. Although not directly stated it may follow that Lys79 *i.e.* the incoming ligand is itself the trigger as has been proposed elsewhere [19]. In hCc, Lys79 unlike Lys73 (the other coordinating residue) is H-bonded between the backbone carbonyl of Ser47 and its side chain Nε amine, thus stabilising and creating a link between the two Ω-loops (Fig. 1). This H-bond is proposed to increase the p$K_a$ of the Lys79 amine to ~ 12 *i.e.* the experimentally determined p$K_{trig}$ (Table 2) [35]. Deprotonation of this H-bonded amine group may now change the dynamics of the Ω-loops and enhance the propensity to dissociate the Met80 ligand, with the deprotonated Lys79 now able to coordinate the ferric heme. In this model, variants in the 40-57 Ω-loop that alter the H-bond pattern, and themselves change the dynamics of the loops, result in disruption of the H-bond between Lys79 and the carbonyl of Ser47, that in turn leads to the drop in the p$K_a$ of the Lys, which is reflected in the lower trigger p$K_a$ of the G41S and Y48H variants (Table 2). However, a significant counter argument against Lys79 as the

trigger is that removal of its titratable amine group by chemical modification leaves the apparent p$K_a$ of the alkaline transition essentially unchanged [20, 21]. On this basis, we favour as discussed, deprotonation within a H-bonded unit that disrupts the linkage between the two Ω-loops. Additional support for this view is found from the p$K_{trig}$ of 10.8 determined for the K79A variant of yeast iso-1 Cc [14], similar to our observations for the disease variants. Therefore, removing Lys79 can be interpreted as disrupting the communication between the two Ω-loops leading to the perturbation of the unit that governs the p$K_{trig}$ (see above).

Deprotonation of the proximal His18, to generate a histidinate species, has also been suggested to be the trigger [15, 22, 23, 67]. Whereas we can't discount this possibility, beyond noting that it does not account for data such as the stopped-flow FT-IR measurements implicating a HP referred to above, and, as Rosell et al. [14] note, it does not account either for data acquired with position 82 variants, we would rather retain this group for consideration as the titratable group responsible for the second deprotonation step and formation of the HS heme species (*vide infra*).

Both optical and EPR spectroscopy demonstrate that at pH values > 10 a HS heme species is present. The kinetic data for the WT and 71-85 Ω-loop variants presented in Figure 7B are consistent with Scheme 2 and are in full agreement with Englander and colleagues [21], who suggest that the transition to the HS heme form proceeds via exposure through a conformational change of a hidden group, which on deprotonation forms a HS heme species that subsequently decays by Lys binding to the ferric heme ion. The conformational change that exposes the group is unknown. However, for simplicity, and because we are seeking to stabilise a HS form, we suggest that the conformational transition that is seen in the WT protein leads to the dissociation of the Met80 ligand (Fig. 9). We envisage that this conformational change, leading to a pentacoordinate HS heme form in ferriCc, is the same one allowing $N_3^-$ binding to the ferric heme. Under this model, dissociation of the Met80 exposes a group, which once deprotonated stabilises the HS heme form (this sequence of events is as depicted with silver arrows in the cube (Fig. 9)). Gadsby et al.[23] have determined indirectly through EPR and MCD spectroscopy that the proximal His18 heme ligand has a p$K_a$ of 11 in the hexacoordinate (His/Met) form of ferriCc. Deprotonation of this group has a powerful *trans* effect on the Fe(III)-S(Met80) bond leading to dissociation and formation of a pentacoordinate form. We propose a reciprocal argument; namely, that the Met80 association/dissociation equilibrium in state III ferricCc leads to a population of pentacoordinate form in which the p$K_a$ of the His18 is lowered. Thus, the mechanism

depicted in Scheme 2 and in the cube proceeds via dissociation of Met80 and stabilisation of the resulting HS species by deprotonation of the coordinated His18 with a $pK_a$ now lowered to ~ 9 for the WT and the 71-85 $\Omega$-loop variants (Fig. 7A). Note that such low $pK_a$ values for ionisation of Fe(III) bound histidines to histidinate have been observed in other heme proteins such as cytochrome $c'$ [68] and *E. coli* cytochrome $b_{562}$ [69]. For the G41S and Y48H variants the mechanism is changed and direct deprotonation of the coordinated His18, prior to Met80 dissociation must occur (Fig. 7A). Bowler and colleagues have structurally illustrated that a non-native state of Cc can generate a water channel involving the 40-57 $\Omega$-loop, allowing access to the proximal His18 ligand [48] and our NMR data support this view of dynamic access to the proximal His18 through the increased dynamics in the 40-57 $\Omega$-loop [9, 10]. Such direct deprotonation of the His18 in the His/Met state would have a $pK_a$ ~11 [23], in keeping with the observed $pK_{a2}$ for the G41S and Y48H variants.

The functional significance of the alkaline transition of Cc may be related to peroxidatic function by examination of Fig. 9. Peroxidase activity requires a pentacoordinate form and thus any of the four species populating the front face of the cube are candidates for this role. As our peroxidase activities were determined at pH 6.5 the major species will be protonated and thus one candidate is the H-pCc-Htrig (Fig. 9). This species certainly is more readily accessed in the two disease variants as demonstrated by relatively rapid $N_3^-$ binding and high peroxidase activity [9, 10]. Furthermore, the disease variants have a lower $pK_{695}$ [9, 10], which implies greater access to the species pCc-H and as Lys is more protonated at this lower pH we may expect more of this pentacoordinate species at equilibrium than in the WT protein. The role (if any) played by the second ionisation ($pK_{a2}$; His18) is more difficult to ascertain. For example, the population of species pCc-H$_{trig}$ depends upon $pK_{a2}$ values (equilibria attained instantly) and the conformational equilibrium (equilibria attained slowly). It is clear experimentally however that where we see this putative HS species in pH jump experiments, it is always at a higher concentration in the G41S and Y48H variants than in the WT protein (as seen by optical and EPR meausrements). Thus, although it is difficult to pinpoint which pentacoordinate forms are responsible for peroxidase activity at a given pH, the disease variants always have a higher population of pentacoordinate forms and thus greater peroxidase activity.

**CONCLUSION**

In our discussion of the alkaline transition we have chosen to frame our thoughts in terms of a H-bonded unit which may be disrupted by deprotonation leading to a reorganisation of the protein structure in order to minimise the free energy of the system. This approach is not in conflict necessarily with the views of Englander and colleagues, who argue that there need not be a specific triggering group in a kinetic sense [35]. However, it is agreed by all literature that a deprotonation, preceding any conformational change, with an intrinsic p$K_a$ ~12 is an essential feature of the alkaline transition. Although, arguments that it is the deprotonation of the incoming Lys ligand may be all that is required to compete for the sixth coordination position and hence initiate the global transition, it is our view that this is difficult to make compatible with results showing that modifications of possible Lys groups so they may not act as ligands leave the alkaline transition relatively unperturbed. Furthermore, a mechanism where an incoming deprotonated lysine stabilises a pre-existing minor pentacoordinate form (through binding) appears not to be consistent with the pH jump experiments which show that deprotonation precedes conformational change. Moreover, our results on the 40-57 Ω-loop variants show that the intrinsic p$K_a$ measured by pH jump is decreased by 1 pH unit. Bearing this in mind, it is immediately apparent from a structural viewpoint how this could be achieved through disruption of the H-bonded network that incorporates the Met80, Tyr67/wat166, Asn52, Thr78 and HP unit.

**SUPPORTING INFORMATION**

Experimental procedure for preparing the I81A, V83G and I81A/V83G variants of hCc, ustification for an invariant $K_D$ in the interpretation of azide binding kinetics, dependence of amplitudes from pH jump stopped-flow experiments and determination of high spin ferric heme concentration by EPR spectroscopy. Table S1, average and standard deviations of the concentrations of the high spin and low spin ferric heme forms in carboxymethyl cytochrome *c* at different pH values. Figure S1 correlations between the thermodynamic and kinetic parameters governing azide binding to hCc and variants. Figure S2 amplitude of absorbance changes following pH jump experiments with hCc and the Y48H variant. Figure S3, low temperature EPR spectra of 150 μM carboxymethyl cytochrome *c* at different pH values.

Figure S4, the pH dependence of the high spin and low spin ferric heme forms in carboxymethyl cytochrome *c*.

**REFERENCES**

[1] Moore, G. R., and Pettigrew, G. W. (1990) Cytochrome c: Evolutionary, Structural and Physicochemical Aspects, *Springer-Verlag, London*.

[2] keilin, D. (1925) On cytochrome, a repiratory pigment, common to animals, yeast and higher plants, *Proc. R. Soc. Lond. B. Biol. Sci. 98*, 312-339.

[3] Alvarez-Paggi, D., Hannibal, L., Castro, M. A., Oviedo-Rouco, S., Demicheli, V., Tortora, V., Tomasina, F., Radi, R., and Murgida, D. H. (2017) Multifunctional Cytochrome c: Learning New Tricks from an Old Dog, *Chem Rev 117*, 13382-13460.

[4] Ow, Y. P., Green, D. R., Hao, Z., and Mak, T. W. (2008) Cytochrome c: functions beyond respiration, *Nat Rev Mol Cell Biol 9*, 532-542.

[5] Huttemann, M., Pecina, P., Rainbolt, M., Sanderson, T. H., Kagan, V. E., Samavati, L., Doan, J. W., and Lee, I. (2011) The multiple functions of cytochrome c and their regulation in life and death decisions of the mammalian cell: From respiration to apoptosis, *Mitochondrion 11*, 369-381.

[6] Kagan, V. E., Tyurin, V. A., Jiang, J., Tyurina, Y. Y., Ritov, V. B., Amoscato, A. A., Osipov, A. N., Belikova, N. A., Kapralov, A. A., Kini, V., Vlasova, II, Zhao, Q., Zou, M., Di, P., Svistunenko, D. A., Kurnikov, I. V., and Borisenko, G. G. (2005) Cytochrome c acts as a cardiolipin oxygenase required for release of proapoptotic factors, *Nat Chem Biol 1*, 223-232.

[7] Wang, X. (2001) The expanding role of mitochondria in apoptosis, *Genes Dev 15*, 2922-2933.

[8] Gonzalez-Arzola, K., Diaz-Moreno, I., Cano-Gonzalez, A., Diaz-Quintana, A., Velazquez-Campoy, A., Moreno-Beltran, B., Lopez-Rivas, A., and De la Rosa, M. A. (2015) Structural basis for inhibition of the histone chaperone activity of SET/TAF-Ibeta by cytochrome c, *Proc Natl Acad Sci U S A 112*, 9908-9913.

[9] Karsisiotis, A. I., Deacon, O. M., Wilson, M. T., Macdonald, C., Blumenschein, T. M., Moore, G. R., and Worrall, J. A. R. (2016) Increased dynamics in the 40-57 Omega-loop of the G41S variant of human cytochrome c promote its pro-apoptotic conformation, *Sci Reps 6*, 30447.

[10] Deacon, O. M., Karsisiotis, A. I., Moreno-Chicano, T., Hough, M. A., Macdonald, C., Blumenschein, T. M. A., Wilson, M. T., Moore, G. R., and Worrall, J. A. R. (2017) Heightened dynamics of the oxidized Y48H variant of human cytochrome c increases its peroxidatic activity, *Biochemistry 56*, 6111-6124.

[11] Theorell, H., and Akesson, A. (1941) Studies on cytochrome c, *J Am Chem Soc 63*, 1804-1820.

[12] Hong, X. L., and Dixon, D. W. (1989) NMR study of the alkaline isomerization of ferricytochrome c, *FEBS Lett 246*, 105-108.

[13] Ferrer, J. C., Guillemette, J. G., Bogumil, R., Inglis, S. C., Smith, M., and Mauk, A. G. (1993) Identification of Lys79 as an iron ligand in one form of alkaline yeast iso-1-ferricytochrome c, *J Am Chem Soc 115*, 7507-7508.

[14] Rosell, F. I., Ferrer, J. C., and Mauk, A. G. (1998) Proton-linked protein conformational switching: Definition of the alkaline conformational transition of yeast iso-1-ferricytochrome c, *J Am Chem Soc 120*, 11234-11245.

[15] Margoliash, E., and Schejter, A. (1966) Cytochrome c, *Advs Prot Chem 21*, 113-286.

[16] Wilson, M. T., and Greenwood, C. (1996) *Cytochrome c: A multidisciplinary approach*, University Science Books, Sausilito, CA.

[17] Davis, L. A., Schejter, A., and Hess, G. P. (1974) Alkaline isomerization of oxidized cytochrome c. Equilibrium and kinetic measurements, *J Biol Chem 249*, 2624-2632.

[18] Cherney, M. M., and Bowler, B. E. (2011) Protein dynamics and function: Making new strides with an old warhorse, the alkaline conformational transition of cytochrome c, *Coord. Chem. Rev. 255*, 664-677.

[19] Battistuzzi, G., Borsari, M., De Rienzo, F., Di Rocco, G., Ranieri, A., and Sola, M. (2007) Free energy of transition for the individual alkaline conformers of yeast iso-1-cytochrome c, *Biochemistry 46*, 1694-1702.

[20] Stellwagen, E., Babul, J., and Wilgus, H. (1975) The alkaline isomerization of lysine-modified ferricytochrome c, *Biochim Biophys Acta 405*, 115-121.

[21] Hoang, L., Maity, H., Krishna, M. M., Lin, Y., and Englander, S. W. (2003) Folding units govern the cytochrome c alkaline transition, *J Mol Biol 331*, 37-43.

[22] Pettigrew, G. W., Aviram, I., and Schejter, A. (1976) The role of the lysines in the alkaline heme-linked ionization of ferric cytochrome c, *Biochem Biophys Res Commun 68*, 807-813.

[23] Gadsby, P. M., Peterson, J., Foote, N., Greenwood, C., and Thomson, A. J. (1987) Identification of the ligand-exchange process in the alkaline transition of horse heart cytochrome c, *Biochem J 246*, 43-54.

[24] Schejter, A., Aviram, I., and Sokolovsky, M. (1970) Nitrocytochrome c. II. Spectroscopic properties and chemical reactivity, *Biochemistry 9*, 5118-5122.

[25] Takano, T., and Dickerson, R. E. (1981) Conformation change of cytochrome c. II. Ferricytochrome c refinement at 1.8 A and comparison with the ferrocytochrome structure, *J Mol Biol 153*, 95-115.

[26] Hartshorn, R. T., and Moore, G. R. (1989) A denaturation-induced proton-uptake study of horse ferricytochrome c, *Biochem J 258*, 595-598.

[27] Tonge, P., Moore, G. R., and Wharton, C. W. (1989) Fourier-transform infra-red studies of the alkaline isomerization of mitochondrial cytochrome c and the ionization of carboxylic acids, *Biochem J 258*, 599-605.

[28] Berghuis, A. M., and Brayer, G. D. (1992) Oxidation state-dependent conformational changes in cytochrome c, *J Mol Biol 223*, 959-976.

[29] Berghuis, A. M., Guillemette, J. G., McLendon, G., Sherman, F., Smith, M., and Brayer, G. D. (1994) The role of a conserved internal water molecule and its associated hydrogen bond network in cytochrome c, *J Mol Biol 236*, 786-799.

[30] Rajagopal, B. S., Edzuma, A. N., Hough, M. A., Blundell, K. L., Kagan, V. E., Kapralov, A. A., Fraser, L. A., Butt, J. N., Silkstone, G. G., Wilson, M. T., Svistunenko, D. A., and Worrall, J. A. R. (2013) The hydrogen-peroxide-induced radical behaviour in human cytochrome c-phospholipid complexes: implications for the enhanced pro-apoptotic activity of the G41S mutant, *Biochem J 456*, 441-452.

[31] Krishna, M. M., Lin, Y., Rumbley, J. N., and Englander, S. W. (2003) Cooperative omega loops in cytochrome c: role in folding and function, *J Mol Biol 331*, 29-36.

[32] Maity, H., Maity, M., Krishna, M. M., Mayne, L., and Englander, S. W. (2005) Protein folding: the stepwise assembly of foldon units, *Proc Natl Acad Sci U S A 102*, 4741-4746.

[33] Krishna, M. M., Maity, H., Rumbley, J. N., Lin, Y., and Englander, S. W. (2006) Order of steps in the cytochrome C folding pathway: evidence for a sequential stabilization mechanism, *J Mol Biol 359*, 1410-1419.

[34] Hu, W., Kan, Z. Y., Mayne, L., and Englander, S. W. (2016) Cytochrome c folds through foldon-dependent native-like intermediates in an ordered pathway, *Proc Natl Acad Sci U S A 113*, 3809-3814.

[35] Maity, H., Rumbley, J. N., and Englander, S. W. (2006) Functional role of a protein foldon--an Omega-loop foldon controls the alkaline transition in ferricytochrome c, *Proteins 63*, 349-355.

[36] Diederix, R. E., Ubbink, M., and Canters, G. W. (2002) Peroxidase activity as a tool for studying the folding of c-type cytochromes, *Biochemistry 41*, 13067-13077.

[37] Sutin, N., and Yandell, J. K. (1972) Mechanisms of Reactions of Cytochrome-C - Rate and equilibrium constants for ligand binding to horse heart ferricytochrome c, *J Biol Chem 247*, 6932-6936.

[38] Diederix, R. E., Ubbink, M., and Canters, G. W. (2001) The peroxidase activity of cytochrome c-550 from Paracoccus versutus, *Eur J Biochem 268*, 4207-4216.

[39] Morison, I. M., Cramer Borde, E. M., Cheesman, E. J., Cheong, P. L., Holyoake, A. J., Fichelson, S., Weeks, R. J., Lo, A., Davies, S. M., Wilbanks, S. M., Fagerlund, R. D., Ludgate, M. W., da Silva Tatley, F. M., Coker, M. S., Bockett, N. A., Hughes, G., Pippig, D. A., Smith, M. P., Capron, C., and Ledgerwood, E. C. (2008) A mutation of human cytochrome c enhances the intrinsic apoptotic pathway but causes only thrombocytopenia, *Nat Genet 40*, 387-389.

[40] De Rocco, D., Cerqua, C., Goffrini, P., Russo, G., Pastore, A., Meloni, F., Nicchia, E., Moraes, C. T., Pecci, A., Salviati, L., and Savoia, A. (2014) Mutations of cytochrome c identified in patients with thrombocytopenia THC4 affect both apoptosis and cellular bioenergetics, *Biochim Biophys Acta 1842*, 269-274.

[41] Johnson, B., Lowe, G. C., Futterer, J., Lordkipanidze, M., MacDonald, D., Simpson, M. A., Sanchez-Guiu, I., Drake, S., Bem, D., Leo, V., Fletcher, S. J., Dawood, B., Rivera, J., Allsup, D., Biss, T., Bolton-Maggs, P. H., Collins, P., Curry, N., Grimley, C., James, B., Makris, M., Motwani, J., Pavord, S., Talks, K., Thachil, J., Wilde, J., Williams, M., Harrison, P., Gissen, P., Mundell, S., Mumford, A., Daly, M. E., Watson, S. P., and Morgan, N. V. (2016) Whole exome sequencing identifies genetic variants in inherited thrombocytopenia with secondary qualitative function defects, *Haematologica 101*, 1170-1179.

[42] Ong, L., Morison, I. M., and Ledgerwood, E. C. (2017) Megakaryocytes from CYCS mutation-associated thrombocytopenia release platelets by both proplatelet-dependent and -independent processes, *Br J Haematol 176*, 268-279.

[43] Josephs, T. M., Morison, I. M., Day, C. L., Wilbanks, S. M., and Ledgerwood, E. C. (2014) Enhancing the peroxidase activity of cytochrome c by mutation of residue 41: implications for the peroxidase mechanism and cytochrome c release, *Biochem J 458*, 259-265.

[44] Silkstone, G., Jasaitis, A., Vos, M. H., and Wilson, M. T. (2005) Geminate carbon monoxide rebinding to a c-type haem, *Dalton Trans*, 3489-3494.

[45] Mason, J. M., Bendall, D. S., Howe, C. J., and Worrall, J. A. (2012) The role of a disulfide bridge in the stability and folding kinetics of Arabidopsis thaliana cytochrome c(6A), *Biochim Biophys Acta 1824*, 311-318.

[46] Santoro, M. M., and Bolen, D. W. (1992) A test of the linear extrapolation of unfolding free energy changes over an extended denaturant concentration range, *Biochemistry 31*, 4901-4907.

[47] Thompson, M. K., Franzen, S., Ghiladi, R. A., Reeder, B. J., and Svistunenko, D. A. (2010) Compound ES of dehaloperoxidase decays via two alternative pathways depending on the conformation of the distal histidine, *J Am Chem Soc. 132*, 17501-17510.

[48] McClelland, L. J., Mou, T. C., Jeakins-Cooley, M. E., Sprang, S. R., and Bowler, B. E. (2014) Structure of a mitochondrial cytochrome c conformer competent for peroxidase activity, *Proc Natl Acad Sci U S A 111*, 6648-6653.

[49] Garcia-Heredia, J. M., Diaz-Moreno, I., Nieto, P. M., Orzaez, M., Kocanis, S., Teixeira, M., Perez-Paya, E., Diaz-Quintana, A., and De la Rosa, M. A. (2010) Nitration of tyrosine 74 prevents human cytochrome c to play a key role in apoptosis signaling by blocking caspase-9 activation, *Biochim Biophys Acta 1797*, 981-993.

[50] Rajagopal, B. S., Silkstone, G. G., Nicholls, P., Wilson, M. T., and Worrall, J. A. (2012) An investigation into a cardiolipin acyl chain insertion site in cytochrome c, *Biochim Biophys Acta 1817*, 780-791.

[51] Yin, V., Shaw, G. S., and Konermann, L. (2017) Cytochrome c as a peroxidase: activation of the precatalytic native state by H2O2-induced covalent modifications, *J Am Chem Soc 139*, 15701-15709.

[52] Harbury, H. A., Cronin, J. R., Fanger, M. W., Hettinger, T. P., Murphy, A. J., Myer, Y. P., and Vinogradov, S. N. (1965) Complex formation between methionine and a heme peptide from cytochrome c, *Proc Natl Acad Sci U S A 54*, 1658-1664.

[53] Kihara, H., Saigo, S., Nakatani, H., Hiromi, K., Ikeda-Saito, M., and Iizuka, T. (1976) Kinetic study of isomerization of ferricytochrome c at alkaline pH, *Biochim Biophys Acta 430*, 225-243.

[54] Nold, S. M., Lei, H., Mou, T. C., and Bowler, B. E. (2017) Effect of a K72A mutation on the structure, stability, dynamics, and peroxidase activity of human cytochrome c, *Biochemistry 56*, 3358-3368.

[55] Hasumi, H. (1980) Kinetic studies on isomerization of ferricytochrome c in alkaline and acid pH ranges by the circular dichroism stopped-flow method, *Biochim Biophys Acta 626*, 265-276.

[56] Estell, D. A., Graycar, T. P., and Wells, J. A. (1985) Engineering an enzyme by site-directed mutagenesis to be resistant to chemical oxidation, *J Biol Chem 260*, 6518-6521.

[57] Lei, H., and Bowler, B. E. (2018) Humanlike substitutions to Omega-loop D of yeast iso-1-cytochrome c only modestly affect dynamics and peroxidase activity, *J Inorg Biochem 183*, 146-156.

[58] Martinez, R. E., and Bowler, B. E. (2004) Proton-mediated dynamics of the alkaline conformational transition of yeast iso-1-cytochrome c, *J Am Chem Soc 126*, 6751-6758.

[59] Gu, J., Shin, D. W., and Pletneva, E. V. (2017) Remote perturbations in tertiary contacts trigger ligation of lysine to the heme iron in cytochrome c, *Biochemistry 56*, 2950-2966.

[60] Kroll, T., Hadt, R. G., Wilson, S. A., Lundberg, M., Yan, J. J., Weng, T. C., Sokaras, D., Alonso-Mori, R., Casa, D., Upton, M. H., Hedman, B., Hodgson, K. O., and Solomon, E. I. (2014) Resonant inelastic X-ray scattering on ferrous and ferric bis-imidazole porphyrin and cytochrome c: nature and role of the axial methionine-Fe bond, *J Am Chem Soc 136*, 18087-18099.

[61] Mara, M. W., Hadt, R. G., Reinhard, M. E., Kroll, T., Lim, H., Hartsock, R. W., Alonso-Mori, R., Chollet, M., Glownia, J. M., Nelson, S., Sokaras, D., Kunnus, K., Hodgson, K. O., Hedman, B., Bergmann, U., Gaffney, K. J., and Solomon, E. I. (2017) Metalloprotein entatic control of ligand-metal bonds quantified by ultrafast x-ray spectroscopy, *Science 356*, 1276-1280.

[62] Ying, T., Wang, Z. H., Lin, Y. W., Xie, J., Tan, X., and Huang, Z. X. (2009) Tyrosine-67 in cytochrome c is a possible apoptotic trigger controlled by hydrogen bonds via a conformational transition, *Chem Commun (Camb)*, 4512-4514.

[63] Moss, D., Nabedryk, E., Breton, J., and Mantele, W. (1990) Redox-linked conformational changes in proteins detected by a combination of infrared spectroscopy and protein electrochemistry. Evaluation of the technique with cytochrome c, *Eur J Biochem 187*, 565-572.

[64] Masuch, R., and Moss, D. A. (2003) Stopped flow apparatus for time-resolved Fourier transform infrared difference spectroscopy of biological macromolecules in (H2O)-H-1, *Appl. Spectrosc. 57*, 1407-1418.

[65] Baddam, S., and Bowler, B. E. (2005) Thermodynamics and kinetics of formation of the alkaline state of a Lys 79-->Ala/Lys 73-->His variant of iso-1-cytochrome c, *Biochemistry 44*, 14956-14968.

[66] Bandi, S., Baddam, S., and Bowler, B. E. (2007) Alkaline conformational transition and gated electron transfer with a Lys 79 --> his variant of iso-1-cytochrome c, *Biochemistry 46*, 10643-10654.

[67] Theorell, H. (1941) Studies on cytochrome c IV. The magnetic properties of ferric and ferrous cytochrome c, *J Am Chem Soc 63*, 1820-1827.

[68] Emptage, M. H., Xavier, A. V., Wood, J. M., Alsaadi, B. M., Moore, G. R., Pitt, R. C., Williams, R. J., Ambler, R. P., and Bartsch, R. G. (1981) Nuclear magnetic resonance studies of Rhodospirillum rubrum cytochrome c', *Biochemistry 20*, 58-64.

[69] Moore, G. R., Williams, R. J., Peterson, J., Thomson, A. J., and Mathews, F. S. (1985) A spectroscopic investigation of the structure and redox properties of Escherichia coli cytochrome b-562, *Biochim Biophys Acta 829*, 83-96.

**For Table of Contents use only**

**Naturally occurring disease-related mutations in the 40-57 Ω-loop of human cytochrome *c* control triggering of the alkaline isomerisation**

Oliver M. Deacon, Dimitri A. Svistunenko, Geoffrey R. Moore, Michael T. Wilson, Jonathan A.R. Worrall